Available online at www.sciencedirect.com
ScienceDirect
Polymer 48 (2007) 4492–4502
polymer
www.elsevier.com/locate/polymer

Linear low density polyethylene (LLDPE)/clay nanocomposites. Part I: Structural characterization and quantifying clay dispersion by melt rheology

Ali Durmus [a,*], Ahmet Kasgoz [a], Christopher W. Macosko [b]

[a] Department of Chemical Engineering, Istanbul University, 34320 Avcilar, Istanbul, Turkey
[b] Department of Chemical Engineering and Material Science, University of Minnesota, 421 Washington Avenue, MN 55455, USA

Received 19 April 2007; received in revised form 24 May 2007; accepted 31 May 2007
Available online 7 June 2007

Abstract

In this study, linear low density polyethylene (LLDPE)/clay nanocomposites with various clay content were prepared by melt processing using two different compatibilizers, maleic anhydride grafted polyethylene (PE-*g*-MA) and oxidized polyethylene (OxPE). Effects of structure and physical properties of the compatibilizers on the clay dispersion and clay amount on the microstructure and physical properties of the nanocomposites were investigated. The OxPE was shown to significantly create interfacial interactions between the polymer phase and clay layers. Rheological behavior of the samples was examined by a dynamic oscillatory rheometry in linear viscoelastic region. Percolation threshold (ϕ_p) and corresponding aspect ratio (A_f) values were determined by analyzing the improvement in storage modulus at low frequency region depending on the clay loading. Lower percolation and higher aspect ratio values were obtained for the sample series prepared with the PE-*g*-MA than that prepared with the OxPE. Moreover, fractal size of the clay network above the percolation point was determined by the scaling law for physical gelation of colloidal flocks to quantify clay dispersion depending on the compatibilizer structure. It was found that the PE-*g*-MA yielded better clay dispersion and more exfoliated structure compared to the OxPE. Microstructural characterization of the samples was also characterized by XRD and TEM.

Keywords: Polyethylene nanocomposite; Oxidized polyethylene; Rheology

1. Introduction

In recent years, polymer/clay nanocomposites (PNC) have generated great interests in the polymer industry as a new type of composite material because of their superior properties such as high heat deflection temperature, gas barrier performance, dimensional stability, enhanced mechanical properties, optical clarity and flame retardancy when compared with the pure polymer or composites having conventional fillers. Depending on the interfacial interactions between the polymer chains and clay layers, final structure of a polymer/clay nanocomposite could be exfoliated or intercalated [1].

First PNC was developed by the Toyota (Japan) R&D team about 15 years ago [2]. They reported successfully preparation and physical properties of nylon-6/clay nanocomposites [3–5]. Dispersion of the silicate layers in such type of nylon/clay nanocomposites is well exfoliated due to the strong interactions, specifically hydrogen bonds, between the polar polymer chains and organically modified clay (org-clay) layers as well as in other polar polymers. Afterwards the publications of Toyota researchers, a great research effort and industrial interest have been generated to develop nanocomposite materials with other polymers. But it is very difficult to obtain a well exfoliated nanocomposite structure for non-polar polymers like polyolefins. Thus, some modified polymers having polar

* Corresponding author. Tel.: +90 212 591 24 80; fax: +90 212 473 70 38.
E-mail address: durmus@istanbul.edu.tr (A. Durmus).

0032-3861/$ - see front matter © 2007 Elsevier Ltd. All rights reserved.
doi:10.1016/j.polymer.2007.05.074

groups, called as compatibilizers or interfacial agents, must be introduced in the nanocomposite formulations to increase the interfacial interactions between the clay layers and the polyolefin matrix [1]. The most widely used compatibilizer is maleic anhydride grafted polyolefins. Nanocomposite formation is a very complex phenomenon for the polyolefins even with a compatibilizer. Graft ratio and molecular weight of the compatibilizer, miscibility with the base polyolefin, compatibilizer/nano-filler weight ratio (α) and processing conditions are important parameters for the final structure and physical properties of the nanocomposite. It has been reported that higher maleic anhydride graft ratio onto the compatibilizer or using a high amount of compatibilizer in nanocomposite compositions could cause miscibility problems between the compatibilizer and main polymer phases. Optimum compatibilizer/filler weight ratio (α) has been proposed as 3 in order to achieve a good clay dispersion and physical enhancement for the polyolefin nanocomposites [6,7].

Many studies have been reported on the polypropylene nanocomposites prepared by melt blending using maleic anhydride grafted polypropylenes (PP-*g*-MA) used as compatibilizer [8–13]. Polyethylene-based nanocomposites are much less studied. Although some attempts were reported to create nanocomposites with various grades of polyethylenes and clays both of which were commercially available, only few successful results were obtained due to the chemical structure of the PE [14–16]. Most studies in the field of polyolefin/org-clay nanocomposites were focused on the effects of clay and compatibilizer amount, intercalant structure between the clay layers and processing conditions on nanocomposite properties rather than the structural features of polymeric compatibilizers. In a few studies, some authors offered that low molecular weight reactive compounds can be used successfully as compatibilizer for the polyolefin nanocomposites [17,18]. They proposed that these functional oligomeric compounds can easily diffuse through the clay galleries and cause an extra delamination because they have much higher mobility than the high molecular weight equivalents during the nanocomposite processing.

In this study, we have focused on preparing linear low density polyethylene (LLDPE)/org-clay nanocomposites with improved physical properties for barrier film applications. We have also attempted to use a low molecular weight oxidized polyethylene (OxPE) as compatibilizer. Oxidized polyethylene is a modified, low molecular weight polyethylene that contains various functionalities such as mainly carboxylic acids, esters and ketones. It has been used as processing aid in some polymer and coating formulations. Krupa et al. used a low molecular weight oxidized Fischer–Trops wax ($M_w = 785$ g mol^{-1}) in polyolefin blends and reported the effects of the oxidized wax on the polarity of the system and corresponding thermal and mechanical properties of the oxidized wax/polyolefin blends [19,20]. They found that the 10% weight concentration of the oxidized wax increased the blend polarity 10 times in case of LDPE and 4.5 times for the HDPE, based on the surface free energy measurements [21]. Oxidized polypropylene (OxPP) was also used to enhance compatibility of polypropylene (PP)/nylon6 blends [22].

In this study, org-clay dispersion in LLDPE phase was quantified by the melt state rheological behavior of the samples and also investigated by XRD and TEM studies depending on the compatibilizer structure. Thermal, mechanical and gas permeability properties of these samples will be reported in second part of the study.

2. Experimental

2.1. Materials

Polymers used in this study are listed in Table 1. Linear low density polyethylene (LLDPE) supplied by ExxonMobil (LL3003®) was used as polymer matrix having a number molecular weight (M_n) of 50 kg mol^{-1}. Two commercial compatibilizers, a maleic anhydride grafted polyethylene donated by Crompton (Polybond® 3029) and a low molecular weight oxidized PE donated by Honeywell (AC® 330) were used as compatibilizers. Melt flow index (MFI) values of the LLDPE and PE-*g*-MA are 3.2 g 10 min^{-1} and 4 g 10 min^{-1}, respectively (ASTM D1238, 190 °C, 2.16 kg). Melt viscosity of the AC® 330 was reported as 3600 cps at 150 °C. Hereafter the compatibilizers are denoted as PE-*g*-MA for the Polybond® 3029 and OxPE for the AC® 330. The clay used in this study was a commercial organo-clay supplied from Southern Clay (Cloisite® 20A). Cloisite® 20A is dimethyl dihydrogenated tallow quaternary ammonium (2Me2HT) salt modified montmorillonite (org-clay). The organic content of Cloisite® 20A was reported as 38% by the manufacturer [23].

2.2. Melt processing

Samples were prepared by melt blending in a DACA Mini Compounder, a vertical co-rotating twin screw extruder, with a re-circulation channel. Polymers and org-clay, dried in an air circulating oven at 80 °C overnight, were mixed manually and loaded into the compounder. All batches, weighing 4 g each, were processed at 180 °C with a screw speed of 100 rpm for 15 min under nitrogen. The maximum shear rate for this instrument was estimated to be 60 s^{-1} at 100 rpm. Then the samples were extruded for about 3 min and cooled down to room temperature. Sample compositions varying with the compatibilizer type and org-clay content from 1 phr (part per hundred of the polymer matrix) to 10 phr are listed in Table 2. Different compositions were designated as MA-*x* and OxPE-*x* where *x* represents the clay amount as phr and MA and OxPE represent the compatibilizers, maleic anhydride grafted

Table 1
Some properties of the polymers used

Polymer	M_n	PDI	d (g/cm^3)	Functional group characteristics
LLDPE	50,000	5.5	0.9175	–
PE-*g*-MA	–	–	0.9600	MAH = 1.6
				AN = 18.3
OxPE	2950	3.2	0.9900	AN = 30

MAH: maleic anhydride graft ratio (wt%), AN: acid number (mg KOH/g).

Table 2
Sample compositions

Sample	Polymer	Compatibilizers		Org-clay
	LLDPE	PE-*g*-MA	OxPE	Cloisite 20A (phr)
LLDPE	100			–
C5	95			5
MA-1	97	3		1
MA-2	94	6		2
MA-3	91	9		3
MA-5	85	15		5
MA-8	74	24		8
MA-10	70	30		10
OxPE-1	97		3	1
OxPE-2	94		6	2
OxPE-3	91		9	3
OxPE-5	85		15	5
OxPE-8	74		24	8
OxPE-10	70		30	10

C5: control sample.

polyethylene and oxidized polyethylene, respectively. Compatibilizer/org-clay weight ratio (α) was taken constant as 3 in each composition to provide a constant dispersion state for the org-clay. Mixing torque (Nm) and load (N) values were recorded during the melt processing.

A control sample (hereafter named as C5) having 5 (wt%) org-clay (95 LLDPE/5 Cloisite® 20A) without compatibilizer was also prepared at the same processing conditions.

2.3. Sample characterization

2.3.1. Rheological measurements

Viscoelastic behavior of the nanocomposites were analyzed by a dynamic oscillatory rheometer in the melt state. A controlled strain rheometer (ARES, Advanced Rheometric Expansion System, Rheometric Scientific) equipped with 25 mm diameter parallel plate geometry was employed for the rheological tests. Samples were directly loaded and molded between the plates and rheological tests were carried out at 160 °C with a gap distance of 0.9−1 mm under nitrogen atmosphere. First, strain sweep test was performed from the initial strain value of 0.1 to a final strain value of 100 in percent, with the frequency of 1 rad/s to determine the linear viscolelastic region of the samples. Storage modulus (G') and loss modulus (G'') were recorded as a function of shear strain (γ%).

In frequency sweep test, a small amplitude oscillatory shear, $\gamma = \gamma_0 \sin(\omega t)$, was applied to the samples. Resulting shear stress was recorded as:

$$\sigma(t) = \gamma_0[G'(\omega)\sin(\omega t) + G''(\omega)\cos(\omega t)] \quad (1)$$

and G', G'' and dynamic viscosity (η^*) were measured as a function of angular frequency (ω) in the range of 0.01−100 rad/s at a strain value in the linear viscoelastic region (strain magnitude of 0.02).

2.3.2. Wide angle X-ray diffraction (WAXD)

WAXD method was used to characterize org-clay dispersion in LLDPE. Extruded samples were analyzed by a Bruker-AXS Rapid XRD Microdiffractometer in the 2θ range from 1° to 12° with the steps of 0.02°, at room temperature to obtain microstructural information of the nanocomposites as well as the extent of clay dispersion.

2.3.3. Transmission electron microscopy (TEM)

Clay dispersion in nanocomposite samples was also observed by the transmission electron microscopy (TEM), (JEOL 1210 with an acceleration voltage of 120 kV). Extruded samples were microtomed in the form of very thin slices (<200 nm) by a cryo-microtome with a glass knife (Reichert UltraCut S Ultramicrotome, Model FC-S Cryo) in liquid nitrogen then the slices were imaged in the TEM.

3. Results and discussion

3.1. Torque changes during melt blending

Torque curves of the samples C5, MA5 and OxPE-5 are given in Fig. 1. As shown, torque level of the OxPE-5 is significantly lower than those of C5 and MA-5 samples. Obviously, such difference originates from the low molecular weight and therefore the low melt viscosity of OxPE. Similarly, it was observed that the mixing torque level of MA-5 is also slightly lower than that of C5. This fact probably resulted from the relatively lower molecular weight and melt viscosity of the PE-*g*-MA than those of LLDPE at the processing temperature. Mixing torque of the OxPE-5 slightly increases with time while it exhibits a slight decrease for both C5 and MA-5.

Artzi et al. discussed the melt viscosity and mixing torque behavior of the ethylene vinyl alcohol copolymer (EVOH)/org-clay nanocomposites with and without the compatibilizers (EVA-*g*-MA and LLDPE-*g*-MA) based on the dynamic mixing conditions in a Brabender melt mixer [24]. They reported that the gradual viscosity increase is indicative of more fracturing

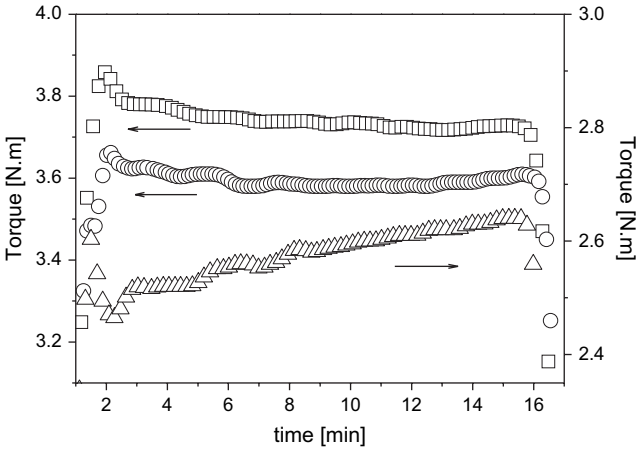

Fig. 1. Torque changes of the samples during melt compounding. Symbols (□), (○) and (△) represent the C5, MA-5 and OxPE-5, respectively.

of the org-clay layers. Increase in mixing torque could reflect on the fracturing of the clay particles into smaller aggregates and undergoing delamination. But in this case, we have mainly deduced that delamination rate can be compared by considering the mixing torque behavior of the nanocomposites prepared with different types of compatibilizers. It is known that interactions between the clay layers and polymer chains and shear forces created in melt blending are major factors in the dispersion of clay in polymer/clay nanocomposites. PE-*g*-MA compatibilizer created a relatively high mixing torque values. On the other hand, compatibilizer–clay affinity should be higher in nanocomposite series prepared with the OxPE than those in the MA series as its –COOH functionality (indicated by the acid number, mg KOH/g) is higher than that of PE-*g*-MA. However, mixing torque of the OxPE-5 sample is much lower than that of MA-5. It can be expected that diffusion of the OxPE chains through the clay galleries is relatively fast due to higher mobility of OxPE chains and relatively high affinity and interactions between –OH groups on the clay surfaces and functional groups of the OxPE. Similar explanation was proposed by Kawasumi et al. for the dispersion mechanism of clay layers in polypropylene (PP) using low molecular weight ($M_w = 30{,}000$ g mol^{-1} and 40,000 g mol^{-1}) oligomeric maleic anhydride grafted polypropylenes (PP-*g*-MA) as compatibilizer [8]. On the other hand, in case of OxPE, it was clearly seen that low M_w compatibilizer (OxPE) cannot yield a high shear value that is required for an effective dispersion of the clay layers into polymer phase. It has been reported that low torque in processing leads to poor clay dispersion in polymer nanocomposites [7,25].

Increase in mixing torque for the nanocomposites series prepared with the OxPE could be explained by the fact that clay layers were gradually delaminated and delamination rate is probably much slower than in the case of relatively higher M_w compatibilizer (PE-*g*-MA). For longer mixing time, mixing torque may reach a plateau as seen in physical gelation. Consequently, although functionality (acid number) of OxPE is higher than that of PE-*g*-MA, it may be expected that the OxPE could yield poor clay dispersion because effective shear forces could not be created during the melt processing.

3.2. Rheological behaviors

3.2.1. Strain dependence of viscoelastic behavior

Rheological behavior of polymer composites in melt state is very critical to understand processability and structure–property relationships for these materials. On the other hand, melt rheology measurements can probe behavior of the relatively large material that is crucial from the macroscopic point of view. In rheological tests, first dynamic strain sweep test was applied to nanocomposite samples in order to characterize strain dependence of the viscoelastic properties of the samples and determine linear viscoelastic (LVE) region. Since the storage modulus (G') is a more sensitive rheological function than the loss modulus (G'') to the structural changes of the nanocomposites, only the storage modulus curves are presented in this study. Dependence of storage modulus (G') on the strain

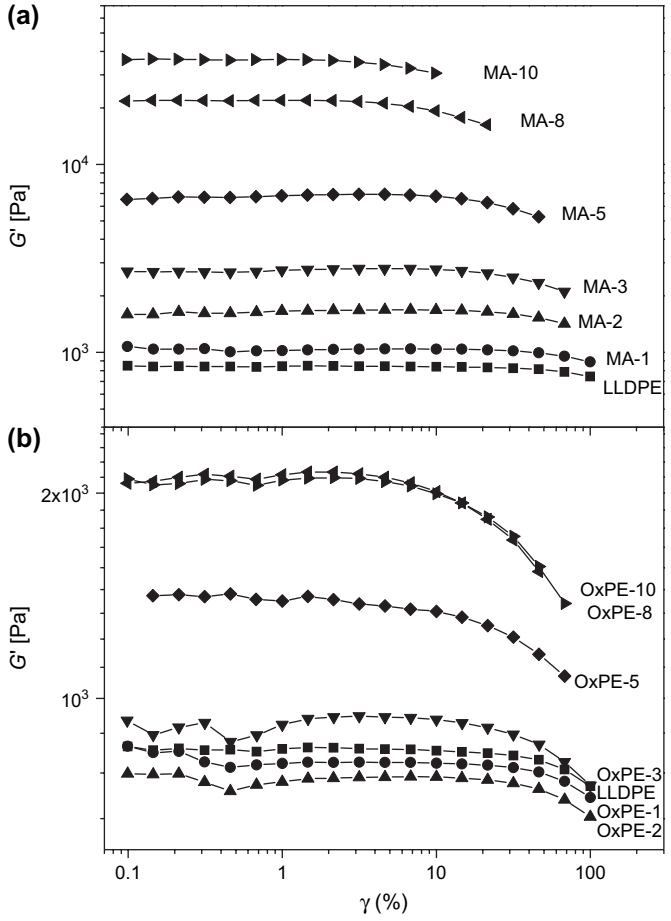

Fig. 2. Storage modulus (G') vs. strain (γ%) curves of the nanocomposites prepared with (a) PE-*g*-MA and (b) OxPE as compatibilizers.

(γ%) for the sample series prepared with the PE-*g*-MA and OxPE is given in Fig. 2. Storage modulus (G') of all the samples exhibits a linear region (Newtonian plateau) at low strains and non-linear region at high strain amplitudes. It was observed that the plateau modulus readily increases with the clay amount for the MA series. But plateau modulus (G'_p) values are lower than modulus of LLDPE for the low clay loaded OxPE-*x* samples. It could be attributed to effects of low molecular weight and low melt viscosity of OxPE at test temperature. Such effect is more pronounced below the org-clay amount of 3 phr which might correspond to network formation (percolation).

Strain dependence of normalized storage modulus ($G'_r = G'/G'_p$) of LLDPE, C5 and the nanocomposite samples, MA-5 and OxPE-5 are shown in Fig. 3. It was observed from the strain sweep test results that deviation from the linear viscoelastic behavior for the nanocomposites starts at lower strains than both LLDPE and C5 samples. Transition point which appeared at the deviation region from the linear to non-linear viscoelastic behavior is defined as critical strain (γ_c). Critical strain value (γ_c) varies with the clay content and dispersion quality depending on the nanocomposite composition. γ_c was generally taken as the strain value at the storage modulus equal to 90% of the plateau modulus (0.9 G').

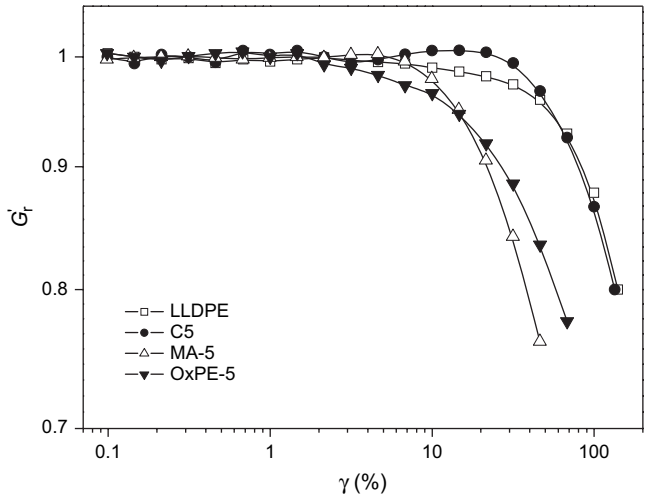

Fig. 3. Normalized storage modulus (G_r') vs. strain (γ%) curves of the LLDPE (□), control sample (●), MA-5 (△) and OxPE-5 (▼) samples.

Plots of the critical strain values against the clay volume fraction (ϕ) are given in Fig. 4 for the samples series. It indicates that the strain limits of linear viscoelastic region of LLDPE/org-clay nanocomposites is very sensitive to clay amount. γ_c values decrease to a strain level of 10% for the high org-clay loaded nanocomposites, however, it is about 80–90% for the LLDPE, C5 and low amount of org-clay loaded samples. OxPE series exhibit higher γ_c values than the PE-*g*-MA series at a given clay amount. These results indicate the microstructural differences in samples and also the effects of compatibilizer type on the the clay dispersion and resulting rheological behavior of the nanocomposites. Moreover, it is observed that the critical strain values display a power law dependency on the volume fraction of clay ($\gamma_c \propto \phi^n$). Power law slopes on a log–log scale were found as −1.1 for the MA series and −0.85 for the OxPE series. Some authors have suggested that strain dependence of clay amount in nanocomposites can be explained by the network formation and by the effects of alignment of the anisotropic clay layers to the strain direction and rupture of some particle–particle interactions of the physical network [26,27].

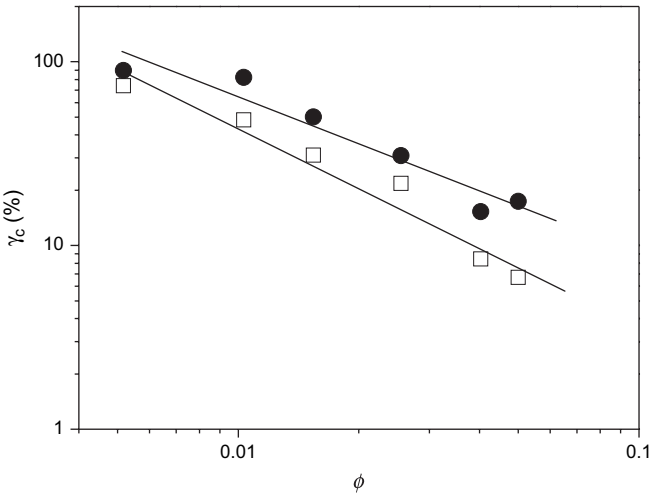

Fig. 4. The dependence of critical strain (γ_c) on the clay volume fraction (ϕ) for the sample series prepared with the PE-*g*-MA (□) and OxPE (●).

3.2.2. Frequency dependence of viscoelastic behavior

Dynamic frequency sweep tests were conducted in linear viscoelastic region ($\gamma = 0.02$) to further study on network formation and microstructural changes of the nanocomposites in detail. First, we compared the rheological behavior of the LLDPE, C5, MA-5 and OxPE-5 samples to understand the effects of the compatibilizer type on the interfacial interactions between the clay layers and polymer chains. Fig. 5 shows the frequency dependence of storage modulus (G') and dynamic viscosity (η^*) of the LLDPE, C5, MA-5 and OxPE-5 samples obtained from the frequency sweep test. It is seen that G' of the MA-5 is the highest in entire range of frequency studied. Especially at low frequency region, it was observed that G' for the MA-5 and OxPE-5 becomes frequency independent which is the characteristic behavior of solid-like materials. Low frequency improvement in G' indicates strong interactions between the clay layers and polymer matrix. This behavior and magnitude of the G' enhancement at low frequency region will be discussed in the following for quantifying clay

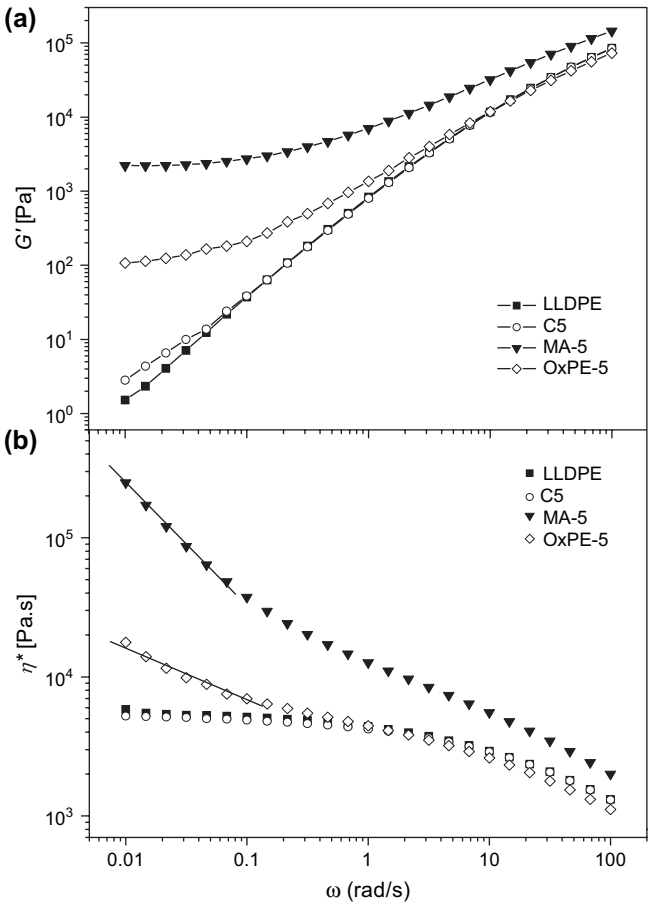

Fig. 5. Comparison of the rheological behavior of the LLDPE, control sample (C5) having 5 phr org-MMT without compatibilizers, MA-5 and OxPE-5. (a) dependence of storage modulus (G') on frequency, (b) dependence of dynamic viscosity (η^*) on frequency.

dispersion. G' values at $\omega = 0.01$ rad/s are 1.5, 2.8, 2230 and 107 Pa for LLDPE, C5, MA-5 and OxPE-5, respectively. These results imply that there is no interaction between the org-clay layers and LLDPE chains, and 5% (wt) of the org-clay cannot show a significant filler effect without a compatibilizer. Thus, C5 sample could be defined as a "macro-composite". On the other hand, considering the G' enhancement at terminal region, it is clearly shown that the OxPE creates a significant interaction at the interface between the polymer and clay layers but this enhancement is lower than the samples prepared with the PE-*g*-MA at a particular org-clay amount. It may be expected that clay layers show better dispersion in MA series than the OxPE series for a given sample composition.

LLDPE and C5 showed a Newtonian plateau in $\eta^*-\omega$ curve (Fig. 5b) at low frequency region which implies that 5 phr of org-clay does not affect the dynamic viscosity of the polymer phase without a compatibilizer. Zero shear rate viscosity (η_0^*) values, obtained experimentally at the frequency of $\omega = 0.01$ rad s^{-1} are 5231 and 5845 Pa s for the C5 and LLDPE, respectively. But it was observed that the dynamic viscosity of nanocomposite samples including 5 phr of org-clay increased dramatically at low frequencies. Increase in viscosity at low frequency region also shows effects of compatibilizer on the interfacial interactions and clay dispersion in polymer phase. Moreover, viscosity curves at low frequency region could be fitted by the power law model. Several authors have used $\eta^*-\omega$ curves to determine power law parameters and explain shear thinning behavior of the polymer nanocomposites at low frequency region [28,29]. For the frequency sweep data, power law expression is written as

$$\eta^* = k\omega^n \tag{2}$$

where η^* is a dynamic viscosity, k is a sample specific pre-exponential factor, ω is the oscillation frequency in the frequency sweep test and n is the shear thinning exponent. k and n can be directly determined from the logarithmic plot of viscosity (η^*) vs. frequency (ω) as

$$\log(\eta^*) = \log k + n\log(\omega) \tag{3}$$

Shear thinning exponent, n, is the slope of straight line obtained by plotting $\log(\eta^*)$ vs. $\log(\omega)$. n is a semi-quantitative measure of the clay dispersion in polymer phase. In this study, power law model was applied to dynamic viscosity (η^*) curves of the samples in low frequency region (between the frequency of 0.1 and 0.01 rad s^{-1}). Power law exponents of the LLDPE, C5, MA-5 and OxPE-5 are listed in Table 3. We can compare the n values for the different nanocomposites prepared at the same composition and processing conditions in order to understand how clay dispersion differs depending on the compatibilizer structure. It is seen that n value of the MA-5 is higher than that of the OxPE-5. It could be expected that the PE-*g*-MA yields better clay dispersion into polymer phase. Eventually, it is also shown that the shear thinning exponent (n) can be used as a measure of degree of clay dispersion depending on the compatibilizer structure.

Table 3
Power law exponents

Sample	$-n$	r^2
LLDPE	0.032	0.9845
C5	0.030	0.9875
MA-5	0.825	0.9979
OxPE-5	0.432	0.9929

Fig. 6(a) and (b) shows the dependence of storage modulus (G') on frequency (ω) for the nanocomposite series of MA and OxPE, respectively, for the various clay loadings. It is clearly seen that org-clay addition influences the storage modulus and this effect is especially more pronounced at low frequencies. As the org-clay amount increases, magnitude of the G' increases and slope of the G' decreases at low frequency region. Especially above a certain fraction of org-clay which is defined as percolation threshold, G' becomes frequency independent ($G' \propto \omega^0$) at low frequency region. This relation is called solid-like (or pseudo solid-like) behavior which indicates strong interactions between the filler and polymer phase. Solid-like behavior was reported for other nanocomposite systems as well [30–34]. Solid-like behavior at low frequency region is primarily due to physical network formation (percolation

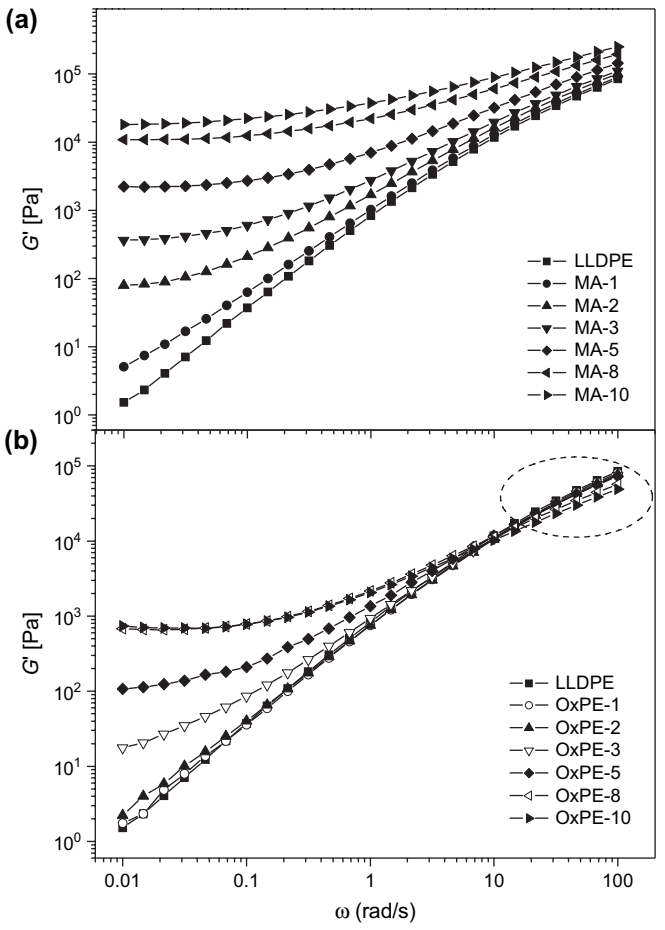

Fig. 6. Storage modulus (G') of the nanocomposites prepared with different compatibilizers: (a) PE-*g*-MA and (b) OxPE.

threshold) of the clay layers at relatively low clay volume fractions. Therefore, better dispersion could yield higher improvement in storage modulus (G') at lower frequencies (plateau modulus, G'_p) for a given weight fraction of the clay since better dispersion provides higher surface area and aspect ratio (A_f).

For the further study on the effects of clay dispersion on the rheological behavior of the nanocomposite samples, increase in storage modulus at terminal region was investigated in more detail. In order to see this enhancement in solid-like plateau modulus more clearly and determine the percolation volume fraction of the clay, the plateau modulus values were plotted (G'_p) in linear scale as a function of the clay volume fraction (ϕ). This relationship is shown in Fig. 7 for the sample series. Two distinct regions where the rheological behavior of the samples changes from the liquid-like to solid-like are noted at these plots. It can also be distinguished that the storage modulus increases dramatically at a certain point of the clay loading. After the critical clay loading, improvement of G'_p exhibits a power law dependence on the clay volume fractions as

$$G'_p \propto (\phi - \phi_p)^{\nu} \tag{4}$$

where ν is the power law constant and ϕ_p is the percolation volume fraction of the clay. When the clay amount is up to 2 phr, G'_p enhances by about 70 times for the MA series of samples compared with the LLDPE matrix. It may be said that in lower clay loadings (<2 phr), rheological properties of the samples are dominated by the polymer phase and exhibit more liquid-like behavior. But in higher clay loadings than about 2 phr, rheologial behavior of the nanocomposites prepared with PE-*g*-MA had a transition from liquid-like behavior to solid-like (or pseudo solid-like) behavior. It is known that this transition can be explained by the formation of the percolation network in polymer/clay nanocomposites [35,36]. Analyzing the rheological behavior of the samples, percolation threshold is found to be about 2 phr (corresponding volume fraction about 0.010) or less for the MA series. On the other hand, improvement in $G'_{\omega=0.01}$ for the OxPE series is about 17 times higher when the clay loading is 3 phr (corresponding volume fraction 0.016) and reaches values more than 70 times higher of the base polymer with the increasing of the org-clay amount (5 phr). It can be expected that percolation threshold is somewhere close to 3 phr for the OxPE series. This result also indicates that clay dispersion in the nanocomposite samples prepared with OxPE is not as good as in the samples prepared with PE-*g*-MA. Critical clay volume fraction (ϕ_p) where the percolation threshold is achieved can be predicted by taking into account this dramatic increase in low frequency modulus as a function of clay loading. Values of ϕ_p were found to be 0.0107 and 0.017 for the MA and OxPE series of the samples, respectively. In Fig. 7, plateau modulus (G'_p) values against the clay volume fraction are plotted with the limited data around the percolation to determine critical clay volume fraction precisely.

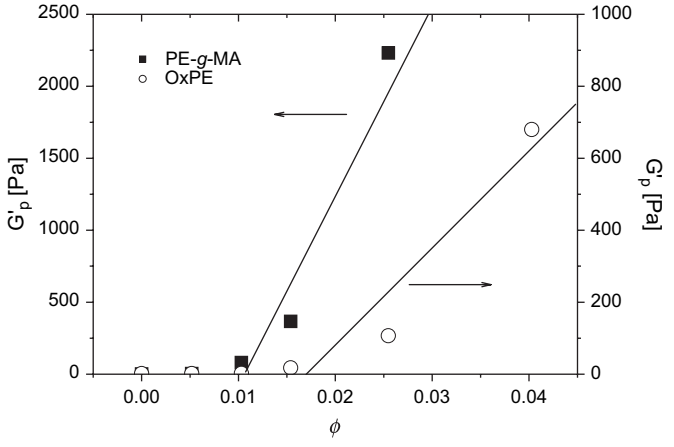

Fig. 7. Plot of the plateau modulus (at $\omega = 0.01$ rad/s) of the sample series as a function of the clay volume fraction. Critical clay volume fraction (ϕ_p) at percolation threshold for the nanocomposite series prepared with PE-*g*-MA (■) and OxPE (○) were obtained by the linear regression through the data.

Obtaining the percolation volume fraction, the aspect ratio of the clay layers (A_f) can be determined. Aspect ratio is known as the ratio of width to thickness of the filler (l/d) and is an indicative parameter which is equal to 1 for spherical particles for filler dispersion in composite systems. In case of polymer–clay nanocomposites, aspect ratio is maximum for the completely exfoliated structures depending on the lateral size of the clay layers. Ren et al. proposed a formula to determine the relationship between the number of clay layers in each tactoid and percolation threshold [30]. This expression can be simplified to calculate the average aspect ratio of the tactoids (A_f) as follows:

$$A_f = \frac{3\phi_{pR}}{4\phi_p} \tag{5}$$

where ϕ_{pR} is the percolation threshold volume fraction for randomly packed spheres and ϕ_p is the experimentally obtained percolation volume fraction [34]. Taking the value of ϕ_{pR} as 0.3 [37] and the values of ϕ_p from Fig. 10, aspect ratio values are determined to be ~21 for the MA series and ~13 for the OxPE series.

Determining the power law dependences of the plateau modulus (G'_p) and critical strain (γ_c) on the clay volume fraction (ϕ), linear viscoelastic properties of the PNCs can also be used to quantify the microstructure of the samples. Shih et al. developed a model to scale elastic properties of the fractal networks which are built up by filler aggregates above the percolation threshold [38]. According to the model, a colloidal gel is described as closely packed fractal flocks. For the nanocomposite systems, it can be considered that the fractal network structure is comprised of the elastically linked filler aggregates. The decrease in the linearity limits of the elastic behavior with the increasing of the filler volume fraction, above the percolation volume fraction of the filler, could be explained by the physical links between the aggregates. Shih et al. named this behavior as strong-link regime. In this regime, power law dependence of critical strain and plateau modulus is described by the following equations:

$$\gamma_c \propto \phi^{-(1+x)/(3-d_f)} \quad (6)$$

$$G'_p \propto \phi^{(3+x)/(3-d_f)} \quad (7)$$

where d_f is the fractal dimension of the filler aggregate network and x is an exponent related to the filler volume fraction and the aggregate size. Power law constants (n) of critical strain were determined as -1.1 and -0.85 for the sample series of MA and OxPE, respectively. Power law constants (ν) for the G'_p dependence on the clay volume fraction above the percolation point are found to be 3.48 and 3.34 for the MA and OxPE series of samples, respectively. Using these power law relationships, Eqs. (6) and (7) were solved simultaneously to give $d_f = 2.17$ for the MA samples and $d_f = 2.32$ for the OxPE samples. Calculated d_f values suggest better clay dispersion with a more open fractal structure for the samples prepared with the PE-*g*-MA compatibilizer as compared to the samples prepared with the OxPE.

Fig. 8(a) and (b) shows the η^* vs. ω curves for the nanocomposite series prepared with the PE-*g*-MA and OxPE used as compatibilizers, respectively. Especially, when the clay loading is high or in the presence of good clay dispersion, dynamic viscosity (η^*) of the nanocomposites shows a dramatic increase and a shear thinning behavior at low frequencies. As shown in viscosity–frequency curves (η^*–ω) of the nanocomposite samples, low amount of clay loaded samples (~2–3 phr) exhibited Newtonian behavior even at low frequencies like unloaded sample (LLDPE). But when the clay amount is increased, dynamic viscosity of the samples increases dramatically and power law behavior becomes dominant at low frequency region. On the other hand, another phenomenon is clearly seen at high frequency region. Generally, increase in clay amount slightly enhances the high frequency modulus ($G'_{\omega=100}$) and viscosity ($\eta^*_{\omega=100}$) of PNC materials. This increase can also be used to analyze the clay dispersion by several rheological models, quantitatively. In contrast with the low frequency behavior of PNCs which resulted due to a physical network formation by the clay layers or aggregates mentioned above, high frequency modulus and viscosity are generally dominated by the polymer matrix. Our results show that high frequency modulus and viscosity readily decrease with the increasing of org-clay for the OxPE series, as the amount of compatibilizer also increases with the clay content [see Fig. 8(b)]. At a frequency of 1 rad/s, a crossover is seen and then elastic behavior of the samples becomes dominant. Nevertheless, it can be concluded that high frequency behavior of the PNCs is especially crucial for the materials prepared with non-polar polymers like polyolefins, rubbers etc. and the relatively low molecular weight compatibilizers.

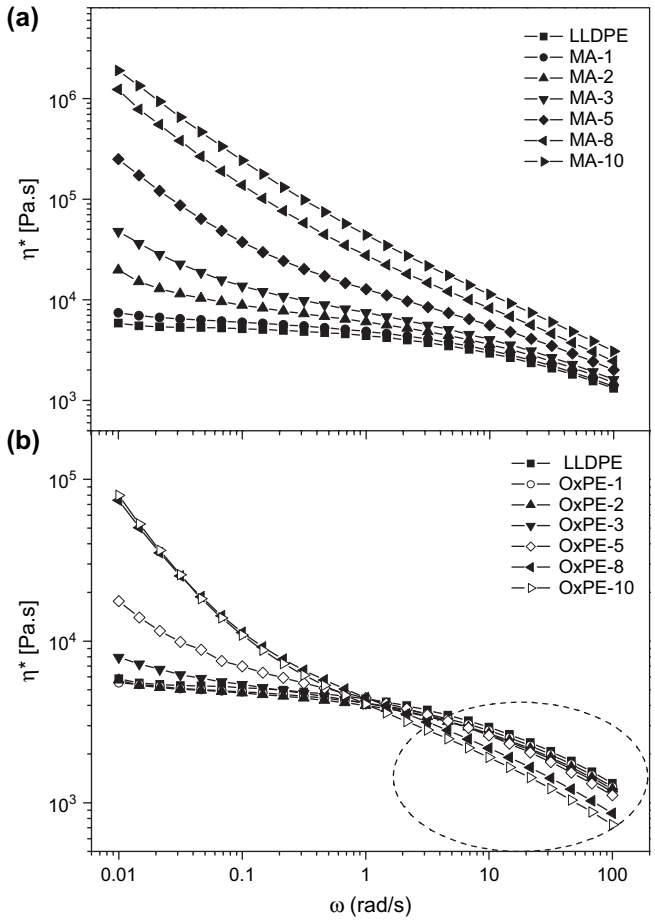

Fig. 8. Frequency dependence of the dynamic viscosity (η^*) of the nanocomposite series prepared with the PE-*g*-MA (a) and OxPE (b) as compatibilizers.

3.3. X-ray diffraction

XRD patterns of the org-clay (Cloisite® 20A), MA-5 and OxPE-5 samples are given in Fig. 9(a). Two diffraction peaks are observed for the org-clay corresponding to basal spacing of $d_{001} = 2.28$ nm ($2\theta = 3.88°$) and $d_{002} = 1.2$ nm ($2\theta = 7.32°$) by using the Bragg equation ($\lambda = 2d\sin\theta$, where λ is the wave length, 0.154 nm, θ is the diffraction angle and d is the basal space between clay layers), respectively. As shown in Fig. 9(a), a very broad peak at about $2\theta = 2.8°$ which could be attributed to d_{001} of the org-clay was observed in the MA-5 sample. This broad peak indicates that most clays are exfoliated but there exist some unexfoliated clay tactoids. But d_{002} peak of the org-clay is not observed in the samples prepared with the PE-*g*-MA. On the other hand, d_{001} and d_{002} peaks are also clearly observed for the OxPE-5, but shifted to lower angles which indicate increase of the d space. Visible and shifted peaks suggest that relatively large stacks of clay platelets are still present in OxPE-5 sample showing clay layers being not completely exfoliated. d_{001} value was calculated as 3.4 nm ($2\theta = 2.61$) for the OxPE-5 which indicated the existence of intercalated tactoids.

Fig. 9(b) shows XRD patterns of the samples prepared with various clay amounts using the OxPE as compatibilizer. Although the peak intensity was increased with the increasing of clay loading, any further shift was not observed in XRD patterns of the OxPE series. This result shows that there exist no difference in clay dispersion and microstructure of

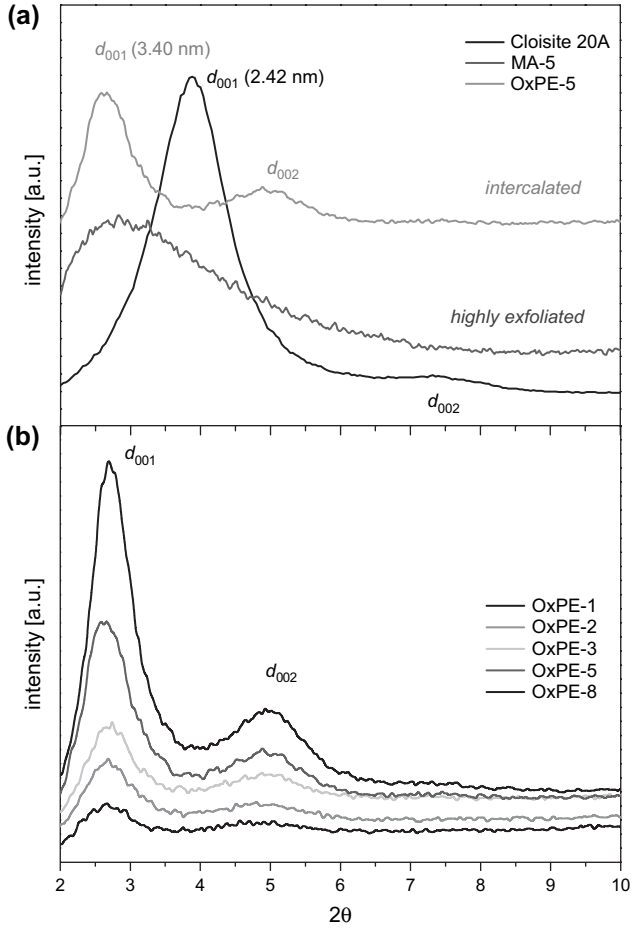

Fig. 9. XRD patterns of the nanocomposites: (a) Cloisite 20A, MA-5 and OxPE-5, (b) samples prepared with various clay amounts using OxPE as compatibilizer.

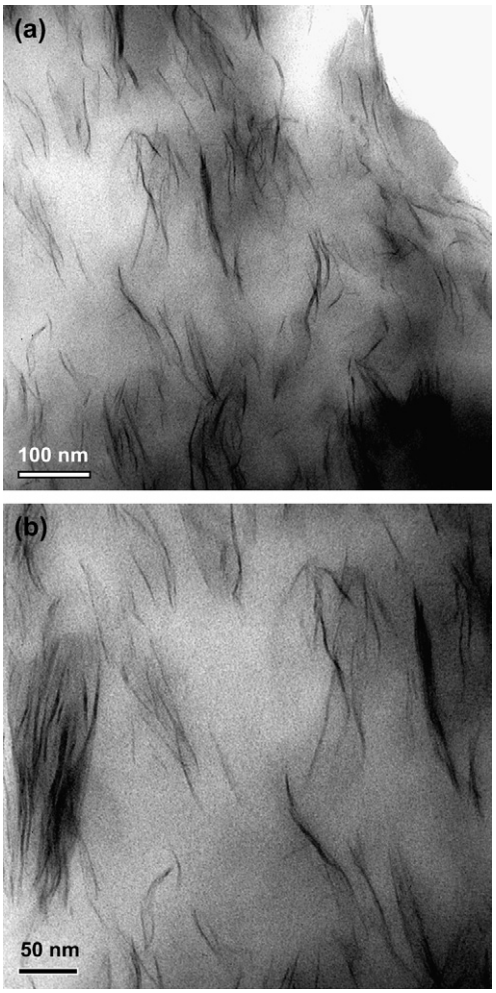

Fig. 10. TEM images of MA-5 sample.

the nanocomposites as the compatibilizer/org-clay weight ratio was taken as constant ($\alpha = 3$) in all compositions.

3.4. TEM study

Effects of the compatibilizer type on the clay dispersion and the resulting morphology of the nanocomposites are shown in TEM images of the MA-5 and OxPE-5 samples given in Figs. 10 and 11, respectively. Clay layers exhibited better dispersion in nanocomposite sample prepared with the PE-*g*-MA as predicted by the melt rheological behavior and XRD analysis of these samples. However, some unexfoliated clay tactoids are shown. Samples prepared with the PE-*g*-MA exhibits more likely a combination of exfoliated/intercalated mixed morphology. On the other hand, OxPE-5 sample has large clay tactoids which correspond to intercalated structure. It is clearly seen that aspect ratio of the clay layers in MA-5 is higher than the aspect ratio in OxPE-5. These morphological observations by TEM were very consistent with the XRD and rheological characterizations of the nanocomposite samples and the aspect ratio estimations based on the percolation volume fraction.

4. Conclusion

Linear low density polyethylene (LLDPE)/org-clay nanocomposites were prepared by melt processing using two different types of compatibilizers, maleic anhydride polyethylene (PE-*g*-MA) and low molecular weight oxidized polyethylene (OxPE). Clay dispersion was investigated by the rheological behavior of the samples depending on the compatibilizer structure, clay amount and interfacial interactions between the clay layers and polymer chains. Increases in storage modulus and dynamic viscosity which indicate a deviation from the sample behavior from viscoelastic-liquid to elastic-solid in terminal region were analyzed in detail. Percolation volume fractions (ϕ_p) of the org-clay were found to be 0.010 and 0.016 for the MA and OxPE series, respectively, taking into account the enhancement in solid-like plateau modulus (G'_p). Corresponding aspect ratio (A_f) values of clay tactoids were calculated as 21 and 13 for the MA and OxPE series, respectively. Assuming the physical gelation of the clay aggregates above the percolation threshold, fractal size of the clay network in the nanocomposite series was determined. Fractal scaling model showed that better clay dispersion was achieved

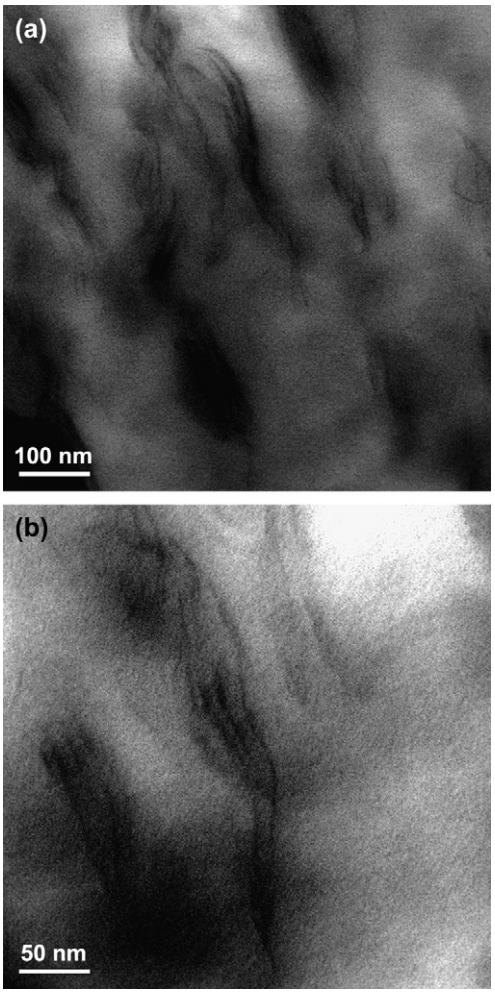

Fig. 11. TEM images of OxPE-5 sample.

with the PE-*g*-MA than OxPE used as compatibilizer. This result was also confirmed by TEM and XRD characterizations of the samples. Nanocomposites prepared with the OxPE showed that there mainly existed intercalated tactoids although the OxPE had higher functionality (corresponding acid number in mg KOH/g) than that of maleic anhyride grafted counterpart. But interestingly, we found that nanocomposite films prepared with the OxPE as compatibilizer showed better barrier properties against O_2 permeability than those prepared with MA-*g*-PE at the same sample composition. These results on the improvement of the gas permeability properties of nanocomposite films will be reported in another publication, Part II: Thermal, mechanical and barrier properties, which is the continuation of the current work.

As a consequence, it was shown that low molecular weight oxidized polyolefins which are commercial and easily accessible modified polyolefins could be used as a new type of compatibilizer to prepare polyolefin/clay nanocomposites by melt processing. Furthermore, rheological analysis of nanocomposites offers a realistic picture to evaluate clay dispersion and microstructure of materials by testing a large amount of sample distinctively and dependence of low frequency modulus on clay loading can be used to quickly assess dispersion quality compared to other structural characterizations.

Acknowledgements

This study was supported by the Research Fund of Istanbul University (Project number: 225/29042004) and the authors appreciate Michail Dolgovskij for his efforts in TEM studies. The authors also thank ExxonMobil, Crompton, Honeywell and Southern Clay companies for supplying various materials used in this work.

References

[1] Ishida H, Campbell S, Blackwell J. Chem Mater 2000;12:1260–7.
[2] Kojima Y, Usuki A, Kawasumi M, Okada A, Fukushima Y, Kurauchi T, et al. J Mater Res 1993;8:1185–9.
[3] Usuki A, Koiwai A, Kojima Y, Kawasumi M, Okada A, Kurauchi T, et al. J Appl Polym Sci 1995;55:119–23.
[4] Kojima Y, Usuki A, Kawasumi M, Okada A, Kurauchi T, Kamigaito O, et al. J Polym Sci Part B Polym Phys 1994;32:625–30.
[5] Kojima Y, Usuki A, Kawasumi M, Okada A, Kurauchi T, Kamigaito O, et al. J Polym Sci Part B Polym Phys 1995;33:1039–45.
[6] Kim KN, Kim HS, Lee JW. Annu Tech Conf Proc 2000;58:3782–5.
[7] Wang Y, Chen FB, Wu KC. J Appl Polym Sci 2005;97:1667–80.
[8] Kawasumi M, Hasegawa N, Kato M, Usuki A, Okada A. Macromolecules 1997;30:6333–8.
[9] Benetti EM, Causin V, Marega C, Marigo A, Ferrara G, Ferraro A, et al. Polymer 2005;46:8275–85.
[10] Zhang YQ, Lee JH, Rhee JM, Rhee KY. Compos Sci Technol 2004;64:1383–9.
[11] Giannelli W, Ferrara G, Camino G, Pellegatti G, Rosenthal J, Trombini RC. Polymer 2005;46:7037–46.
[12] Szazdi L, Pukanszky Jr B, Földes E, Pukanszky B. Polymer 2005; 46:8001–10.
[13] Wang Y, Chen FB, Li YC, Wu KC. Composites Part B 2004;35:111–24.
[14] Hotta S, Paul DR. Polymer 2004;45:7639–54.
[15] Chrissopoulou K, Altintzi I, Anastasiadis SH, Giannelis EP, Pitsikalis M, Hadjichristidis N, et al. Polymer 2005;46:12440–51.
[16] Lee JH, Jung D, Hong CE, Rhee KY, Advani SG. Compos Sci Technol 2005;65:1996–2002.
[17] Kato M, Usuki A, Okada A. J Appl Polym Sci 1997;66:1781–5.
[18] Hasewaga N, Kawasumi N, Kato M, Usuki A, Okada A. J Appl Polym Sci 1998;67:87–92.
[19] Krupa I, Luyt AS. Polymer 2001;42:7285–9.
[20] Krupa I, Luyt AS. Polym Degrad Stab 2001;73:157–61.
[21] Novak I, Krupa I, Luyt AS. J Appl Polym Sci 2005;95:1164–8.
[22] Abdouss M, Sanjani NS, Azizinejad F, Shabani M. J Appl Polym Sci 2004;92:2871–83.
[23] http://www.scprod.com/product_bulletins/PB%20Cloisite%2020A.pdf.
[24] Artzi N, Narkis M, Siegmann A. J Polym Sci Part B Polym Phys 2005;43:1931–43.
[25] Wang Y, Chen FB, Wu KC, Wang JC. Polym Eng Sci 2006;46:289–302.
[26] Khrisnamoorti R, Ren J, Silva AS. J Chem Phys 2001;114(11):4958–78.
[27] Wan T, Clifford MJ, Gao F, Bailey AS, Gregory DH, Somsunan R. Polymer 2005;46:6429–36.
[28] Wagener R, Reisinger TJG. Polymer 2003;44:7513–8.
[29] Bellucci F, Camino G, Frache A, Ristori V, Sorrentino L, Iannace S, et al. e-polymer, www.e-polymers.org, 2006. paper no. 14.
[30] Ren J, Silva AS, Krishnamoorti R. Macromolecules 2000;33:3739–46.
[31] Hyun YH, Lim ST, Choi HJ, Jhon MS. Macromolecules 2001;34:8084–93.
[32] Jeon HS, Rameshwaram JK, Kim G, Weinkauf DH. Polymer 2003;44:5749–58.

[33] Zhao J, Morgan AB, Harris JD. Polymer 2005;46:8641–60.
[34] Vermant J, Ceccia S, Dolgovskij MK, Maffettone PL, Macosko CW. J Rheol 2007;51:429–50.
[35] Lim YT, Park OO. Rheol Acta 2001;40:220–9;
J Polym Sci Part B Polym Phys 2004;42:1000–9.
[36] Shen L, Lin Y, Du Q, Zhong W, Yang Y. Polymer 2005;46: 5758–66.
[37] Isichenko MB. Rev Mod Phys 1992;64:961–1043.
[38] Shih WH, Shih WY, Kim SI, Aksay AI. Phys Rev A 1990;42: 4772–9.